Sensors and Materials, Vol. 36, No. 12 (2024) 5577–5590
MYU Tokyo

S & M 3886

Integrative Approaches to Monitoring Cultivated Land Subsidence in Hilly Regions: Applications of Differential Interferometric Synthetic Aperture Radar and Small Baseline Subset Interferometric Synthetic Aperture Radar Technologies

Huang Xinyi,[1] Guo Ming,[1,2] Huang Huimin,[3*] Wang Zhenda,[3]
Wang Ruoxin,[1,2] Wei Yaxuan,[1,2] and Wang Mengru[1]

[1]Beijing University of Civil Engineering and Architecture, School of Geomatics and Urban Spatial Informatics, Beijing 102616, China
[2]International Joint Laboratory of Safety and Energy Conservation for Ancient Buildings, Ministry of Education
[3]Jiangxi Institute of Natural Resources Mapping and Monitoring, Nanchang 330002, China

(Received November 1, 2024; accepted December 16, 2024)

Keywords: D-InSAR, SBAS-InSAR, land subsidence monitoring, Sentinel-1A SAR

In response to the challenges faced in monitoring cultivated land in hilly regions, we take a city as a case study to explore the application of differential interferometric synthetic aperture radar (D-InSAR) and small baseline subset InSAR (SBAS-InSAR) technologies in constructing a spatial database for cultivated land monitoring. The complexity and diversity of cultivated land in hilly regions pose challenges for traditional monitoring methods. These methods often fail to meet the required standards for efficiency and accuracy. Therefore, in this study, we selected 20 Sentinel-1A satellite images captured between October 26, 2022 and May 24, 2024, and employed D-InSAR and SBAS-InSAR technologies for the high-precision monitoring of changes in cultivated land and planting attributes. We processed and analyzed the collected data and then compared the performance of the two InSAR technologies in monitoring cultivated land. We found that the maximum cumulative subsidence values detected in the research area by D-InSAR and SBAS-InSAR were 28 and 8 mm, respectively. D-InSAR technology responds quickly to minor changes in cultivated land. However, it is highly sensitive to noise, especially in hilly regions with large topographic variations. SBAS-InSAR technology effectively reduces atmospheric effects and other sources of error. This approach provides more stable and smoother monitoring results for cultivated land. This technical framework is expected to be extended to more hilly regions in the future. It will contribute to the comprehensive protection and rational use of cultivated land nationwide.

1. Introduction

In hilly regions, cultivated land is the foundation of agricultural production and a crucial part of ecological security. This land supports biodiversity, maintains water cycles, and offers

*Corresponding author: e-mail: 84157165@qq.com
https://doi.org/10.18494/SAM5444

ISSN 0914-4935

habitats for various species. However, it faces growing vulnerability to subsidence due to natural geological phenomena, human engineering activities, and global climate change.

The subsidence of arable land has profound impacts. It reduces soil fertility and disrupts drainage efficiency. This decline directly harms crop yields. In addition, land degradation can damage irrigation systems, which limits water supply for agriculture. These challenges accelerate soil erosion and threaten the stability of agricultural production systems essential to food security. The deterioration of cultivated land disrupts the ecological balance and threatens the sustainability of agricultural practices and environmental health. Traditional techniques, such as ground leveling and global navigation satellite system (GNSS) measurements, provide precise vertical displacement data. However, they face major limitations in complex hilly and mountainous terrains when applied to the challenging task of monitoring farmland settlement. These conventional methods involve cumbersome operational procedures and high costs. They also have a limited monitoring scope. As a result, they are inadequate for large-scale and continuous land subsidence observation.

To address these challenges, synthetic aperture radar interferometry (InSAR) has emerged as a prominent technology for monitoring surface deformation. InSAR offers unique advantages, including all-weather and all-sky capabilities, a wide spatial coverage, and high measurement precision. Differential InSAR (D-InSAR) is particularly effective in detecting millimeter-level surface displacements through the analysis of phase variations in multiple SAR images. However, this technology faces limitations such as atmospheric delays, terrain phase errors, and temporal decorrelation. These issues become more pronounced during long-term monitoring and can compromise accuracy and stability. To overcome these challenges, small baseline subset InSAR (SBAS-InSAR) was developed to improve the reliability of subsidence monitoring. This method optimizes the use of time-series SAR images from multiple short baselines. It effectively mitigates atmospheric disturbances and temporal decorrelation, enhancing the accuracy and continuity of surface deformation monitoring. SBAS-InSAR is particularly suited for the complex conditions of hilly and mountainous regions. Currently, D-InSAR and SBAS-InSAR technologies are widely applied in cultivated land monitoring. Ni and colleagues analyzed surface subsidence in Huaibei City using SBAS-InSAR to identify key influencing factors.(1) Yang utilized SBAS-InSAR technology to monitor surface deformation in the Lijiang River basin.(2) Zhou and his team used SBAS-InSAR to address uplift rail data in the Pingshan mining area. They analyzed the spatiotemporal evolution of deformation using the standard deviation ellipse method.(3) A study on the analysis and prediction of the surface subsidence pattern of the 6306 working face at Dongtan Coal Mine was conducted by Zhu and his team, utilizing D-InSAR technology.(4) Xu and colleagues demonstrated the efficacy of a dam deformation detection and monitoring approach based on SBAS-InSAR technology.(5) Wang employed D-InSAR technology for monitoring land surface settlement in the Pearl River Delta.(6) Guo *et al.* used PSInSAR, SBAS-InSAR, and point cloud modeling to monitor the deformation of an LNG storage tank on a specific island, which revealed consistent deformation rates and localized deformations at the millimeter level.(7) Ma *et al.* processed Sentinel-1A data using D-InSAR and concluded that D-InSAR offers advantages in addressing ground collapse issues.(8) Yan *et al.* obtained extensive surface deformation information in the Ya'an area through the application of

D-InSAR.[9] Wang and his colleagues investigated and compared the applications of D-InSAR and SBAS-InSAR in monitoring ground subsidence in the Jining mining area of Shandong Province.[10] The utilization of InSAR and LiDAR technologies by Guo *et al.* for monitoring the deformation of the Fuwangge Rockery in Qianlong Garden achieved consistent and complementary results, with an expected error within 5 mm.[11] Shi and colleagues proposed a method to monitor and predict mining subsidence. Their method integrates SBAS-InSAR technology with convolutional neural networks and long short-term memory networks.[12] Gu and his team used 60 Sentinel-1A datasets covering Jianshui County to apply SBAS-InSAR technology. This approach enabled them to extract temporal deformation information related to landslides.[13] Yang and his colleagues assessed the feasibility and accuracy of SBAS-InSAR technology in monitoring surface subsidence due to strip mining and confirmed that it met the specified requirements.[14] Wang *et al.* monitored surface settlement in the Honghui mining area using remote sensing and SBAS-InSAR technology to study deformation characteristics.[15] Jin and his team utilized SBAS-InSAR technology to monitor and develop a settlement prediction model for studying the surface settlement at the Gaoyang Coal Mine.[16] Wei and Wang used SBAS-InSAR to analyze deformation along the Xi'an subway and predicted settlement at typical stations.[17] Zhang *et al.* applied D-InSAR and SBAS-InSAR in the Dingji Coal Mine, integrating Kriging interpolation to achieve continuous high-precision settlement results.[18] Huang monitored ground subsidence in the Yungang mining area using D-InSAR, SBAS-InSAR, and Persistent Scatterer Interferometric Synthetic Aperture Radar (PS-InSAR) with Sentinel-1A data.[19] Wu and Hu investigated the feasibility and accuracy of second-track D-InSAR technology for settlement monitoring in a mining area in Zoucheng, Shandong Province. Through comparison with leveling observation data, they verified the technology's high monitoring accuracy and application advantages.[20] Liu and his colleagues studied the application of SBAS-InSAR technology in monitoring ground subsidence in the Heishan mining area. Through time-series interference analysis, they successfully retrieved the distribution of the subsidence center and amounts of settlement.[21] Guoming *et al.* combined PS-InSAR, SBAS-InSAR, and LiDAR technologies to monitor deformation along Xiamen Metro Line 2.[22]

Given the distinctive advantages of D-InSAR and SBAS-InSAR technologies in monitoring cultivated land subsidence, in this study, we focus on hilly regions, with the objective of further exploring the efficacy of these two technologies in practical applications. Through a comparative analysis, we will assess the performance of both technologies in monitoring cultivated land subsidence, specifically examining their accuracy, continuity, and adaptability to complex terrain conditions. Our aim is to provide scientific insights for the protection and management of cultivated land in hilly regions, thereby fostering the harmonious coexistence of sustainable agricultural development and ecological preservation. The field case analysis conducted in this study will offer novel perspectives and technical support for enhancing the cultivated land monitoring technology system in hilly and mountainous regions. It will also facilitate the precise management and long-term, stable utilization of cultivated land resources, ultimately contributing to the sustainable use and conservation of these vital resources.

2. Technical Route

2.1 D-InSAR technical route

The technical roadmap is illustrated in Fig. 1.

The main principles are

$$\varphi = \varphi_{flat} + \varphi_{top} + \varphi_{def} + \varphi_{atm} + \varphi_{noise} + k \times 2\pi , \tag{1}$$

where φ_{flat} is the phase of flat land, φ_{top} is the topographic phase, φ_{def} is the phase caused by the deformation of the line-of-sight (LOS) direction, φ_{atm} is the atmospheric delay phase, φ_{noise} is the noise phase, and k is the ambiguity of the whole week. φ_{flat} can be estimated from the baseline, and φ_{top} can be estimated using the existing DEM.[23]

If the effect of the atmospheric and noise phases is ignored, the interference phase φ_{def} after ground subsidence can be estimated by removing the estimated φ_{flat} and φ_{top}.

$$\varphi_{def} = -\frac{4\pi}{\lambda}\left(R_1 - R_2\right) + \frac{4\pi}{\lambda}\Delta r \tag{2}$$

Here, R_1 is the main oblique distance of the image, R_2 is the oblique distance of the auxiliary image, and Δr is the ground point displacement caused by settlement. The first $-\frac{4\pi}{\lambda}(R_1 - R_2)$ before the plus sign is the interference phase before the deformation. The $\frac{4\pi}{\lambda}\Delta r$ after the plus sign is the deformation phase caused by ground subsidence.

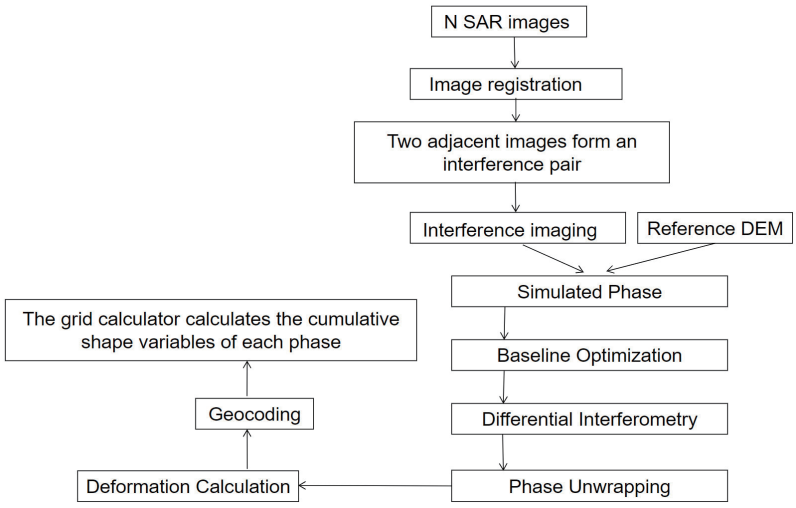

Fig. 1. D-InSAR technology roadmap.

2.2 SBAS-InSAR technical route

The technical roadmap is illustrated in Fig. 2.

With the time-space baseline threshold being set, SBAS-InSAR technology divides the time-series SAR image data that meet the threshold requirements into multiple independent interference subsets with a short spatiotemporal baseline to ensure the coherence of interference pairs and thus obtain more accurate land subsidence monitoring results.

Assuming that the SAR satellite obtains $N + 1$ SAR images of different periods in the research area, k differential interferograms can be obtained by the set time and space thresholds. Then the differential interference phase $\delta\varphi_k$ of the K-image in the azimuth-range pixel coordinate system is shown as

$$\delta\varphi_k(x,y) = \varphi(t_b,x,r) - \varphi(t_a,x,r) \approx \frac{4\pi}{\lambda}\left[d(t_b,x,r) - d(t_a,x,r)\right], \tag{3}$$

where λ is the radar wavelength, t_a and t_b represent the acquisition times of the master and slave images corresponding to the k-th differential interferogram, $\varphi(t_b, x, r)$ and $\varphi(t_a, x, r)$ are the phases of the t_b and t_a moments, and $d(t_a, x, r)$ and $d(t_b, x, r)$ are the cumulative amounts of deformation in the LOS direction of the pixel (x, y) at time t_a and time t_b relative to the initial time t_0, respectively. After removing the terrain residual phase, atmospheric delay phase, and various noise phases, the average rate of land subsidence v^t can be shown as

$$v^t = \left[v_1 = \frac{\varphi_1}{t_1 - t_0}, \ldots, v_n = \frac{\varphi_n - \varphi_{n-1}}{t_n - t_{n-1}}\right]. \tag{4}$$

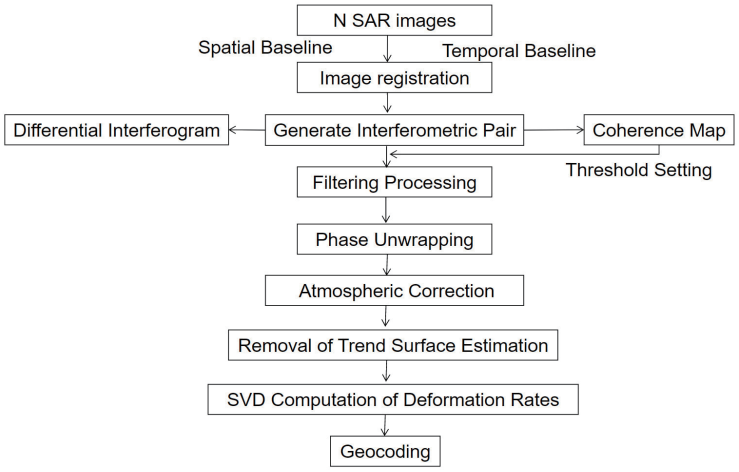

Fig. 2. SBAS-InSAR technology roadmap.

Then the phase is

$$\sum_{E=S_J}^{E_J}(t_k - t_{k-1})v_k = \delta\varphi_j \left(j = 1,2,3,...,n\right), \tag{5}$$

where E_J is main image acquisition time, S_J is the time obtained from the image, and v_k is the pixel deformation rate at time k.

Thus, by combining Eqs. (4) and (5), $A(j, k) = t_k - t_{k-1}$ and A are defined as a rank deficient matrix of $m \times n$, and the matrix equation is obtained as below.

$$Av = \delta\phi \tag{6}$$

Since the matrix is typically rank-deficient, Eq. (6) may not have a unique solution. Therefore, the phase value of the average settlement rate can be obtained by a singular value decomposition method and least squares method. Then the amount of ground settlement can be obtained.[24]

3. Overview of and Data Source for the Study Area

3.1 Study area

The project files with the .psx extension were obtained from UAV surveys and imported into Agisoft PhotoScan. These files contain all project settings, processing steps, and links to the original image files. A preliminary high-resolution color 3D model of the study area was generated based on this data. Figure 3 illustrates the generated model. High-resolution orthophoto TIF files were also produced from the data. These TIF files were imported into ArcMap software. Ground deformation point data obtained through the SBAS-InSAR technique were overlaid on the TIF files. Spatial matching and overlay analysis were performed to identify valid data within the cultivated land areas. The identified regions, shown in Fig. 4, were selected as the focus for subsequent research. Figure 5 shows the geographical location of the study area.

Fig. 3. (Color online) High-resolution color 3D model of the study area constructed from UAV-collected images.

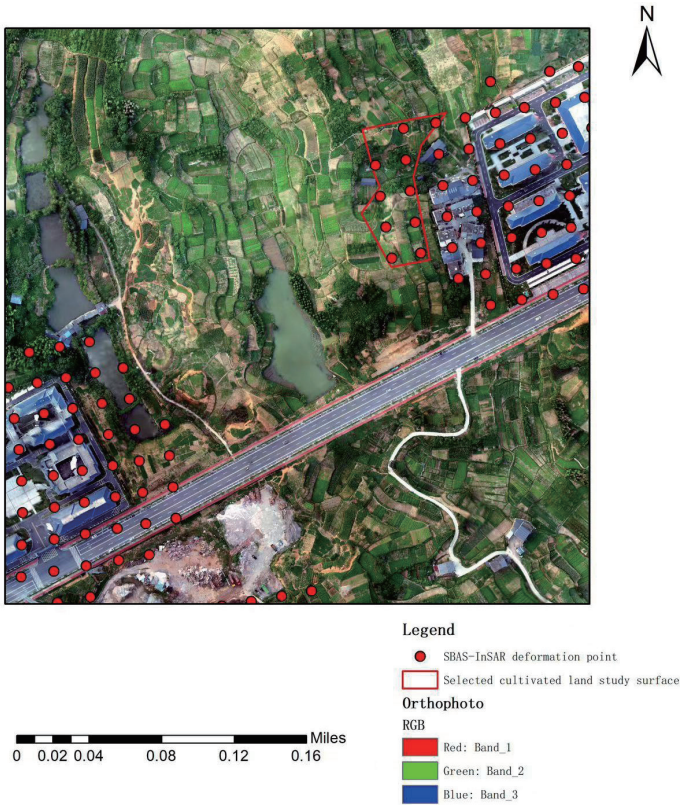

Fig. 4. (Color online) Effective agricultural areas identified by spatial matching and overlay analysis.

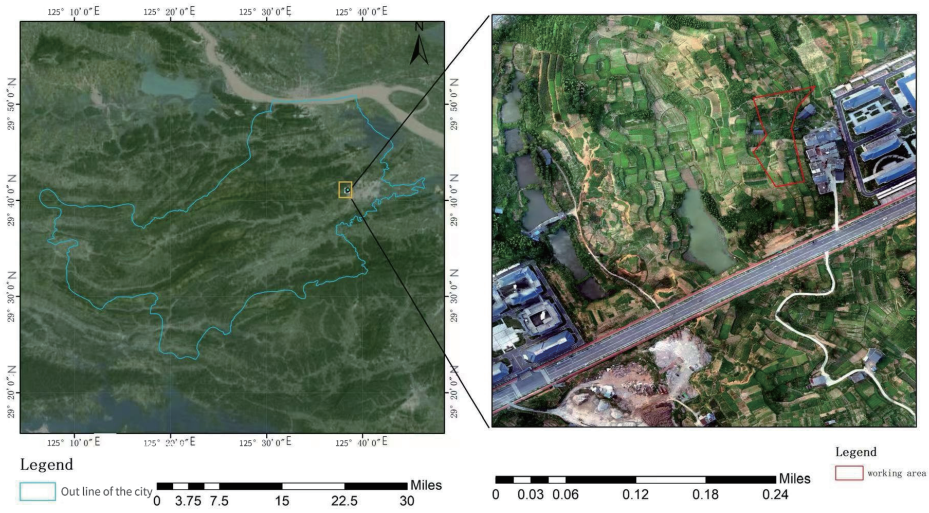

Fig. 5. (Color online) Study area.

3.2 Data collection

To comprehensively evaluate the surface deformation characteristics of the study area, multiple high-resolution remote sensing data and technical methods were utilized. In this study, we aimed to achieve precise monitoring and analysis of surface deformation through multi-source data integration. The following are the primary datasets used in this study and their sources.

(1) SRTM DEM Data: We utilized SRTM DEM data covering the research area. This dataset was generated by NASA's Shuttle Radar Topography Mission. It has a spatial resolution of 30 m and is known for its high accuracy and extensive coverage.
(2) Sentinel-1A Data: This dataset includes 20 scenes of Sentinel-1A VV polarization data for a city. These scenes were collected between October 26, 2022 and May 24, 2024.
(3) UAV Data: UAV data were exported in JPG and PSX formats. These datasets provided additional support for detailed analysis and modeling.

4. InSAR Data Processing

4.1 D-InSAR technology

A total of 20 images were generated between October 26, 2022 and May 24, 2024. Each pair of adjacent images was combined to form 19 interferometric pairs, which were processed sequentially. The hilly area of Jiangxi Province features complex terrain with significant surface undulations and extensive vegetation cover. The diverse vegetation structure and radar wave scattering by vegetation strongly affect the SAR image interference phase. These conditions lead to high phase noise, low backscattering coefficients, weak echo signals, and poor coherence. To suppress the impact of noise on the interference phase, multiview processing of SAR images with a 2:7 ratio is applied. This approach captures small surface deformations and smooths the distance-related interference phase to reduce noise. It enhances the quality of the interference phase in vegetated areas, averages phase noise caused by vegetation scattering, improves interferogram coherence, and maintains high spatial resolution. Goldstein's filtering method is applied for filtering and coherence calculation. The least-cost flow method is used for phase unwrapping. Control points are selected in areas far from the deformation region with high coherence and good phase on the flattened interferogram. The automatic track refinement method is used to calculate track refinement and phase migration. Control points with large errors are removed from the results to perform phase transformation, deformation extraction, and geocoding. The cumulative settlement results obtained by D-InSAR technology in May 24, 2024 are shown in Fig. 6.

4.2 SBAS-InSAR technology

4.2.1 Data processing

A total of 20 SAR images from between October 26, 2022 and May 24, 2024 were selected. The spatial and temporal baseline thresholds were set at 2% of the maximum baseline and 120

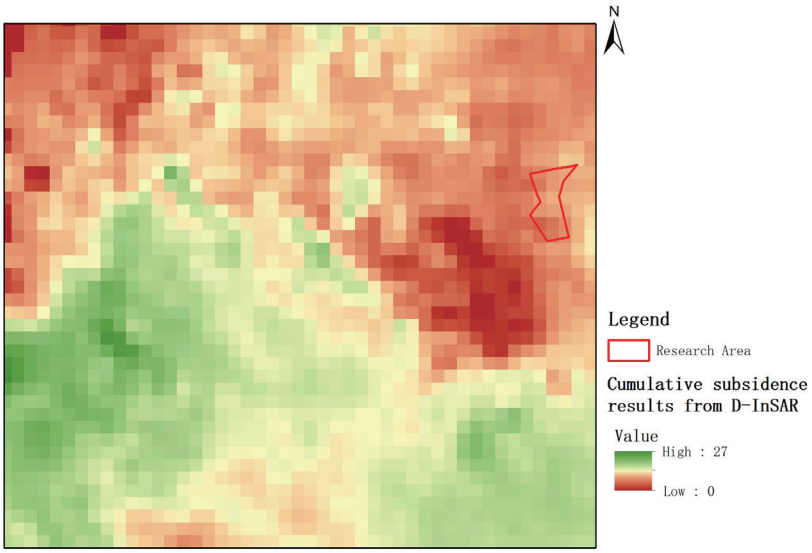

Fig. 6. (Color online) Cumulative subsidence results obtained by D-InSAR.

days, respectively. Interferometric pair combination was conducted, resulting in 40 interference pairs. The spatiotemporal baseline diagram obtained after screening is shown in Fig. 7.

Ground Control Points (GCPs) without residual terrain, deformation fringes, or phase jumps are selected for track refinement and reflattening. The SBAS inversion process begins with estimating the deformation rate and residual terrain using a linear model. Then, time-series displacement is calculated on the basis of the deformation rate with customized atmospheric filtering. Finally, the deformation results are geocoded and projected in the user-defined direction. The cumulative settlement results are obtained by the SBAS-InSAR technology in May 24, 2024 and are shown in Fig. 8.

4.2.2 Increasing the observation point density of SBAS-InSAR deformation results

To improve the accuracy and detail of SBAS-InSAR deformation results, increasing the density of observation points within the cultivated land becomes essential. This enhancement ensures better spatial resolution and more precise monitoring of deformation in relatively flat areas. The following steps outline the approach to refining the observation network and enhancing the reliability of the results.

(1) Data fusion: The identified cultivated land range is spatially matched with the deformation results obtained with SBAS-InSAR to determine the location of InSAR observation points within the cultivated land range.

(2) Observation point encryption: For the cultivated land, the density of observation points can be appropriately increased because of the relatively flat surface and small changes. New observation points are added between existing observation points by interpolation or other methods.

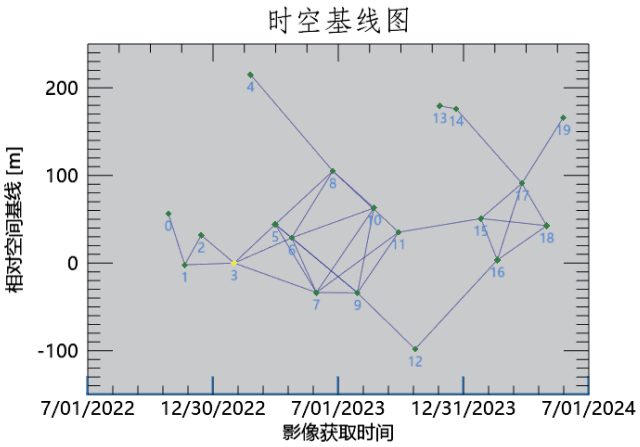

Fig. 7. (Color online) Temporal-spatial baseline map was derived after screening.

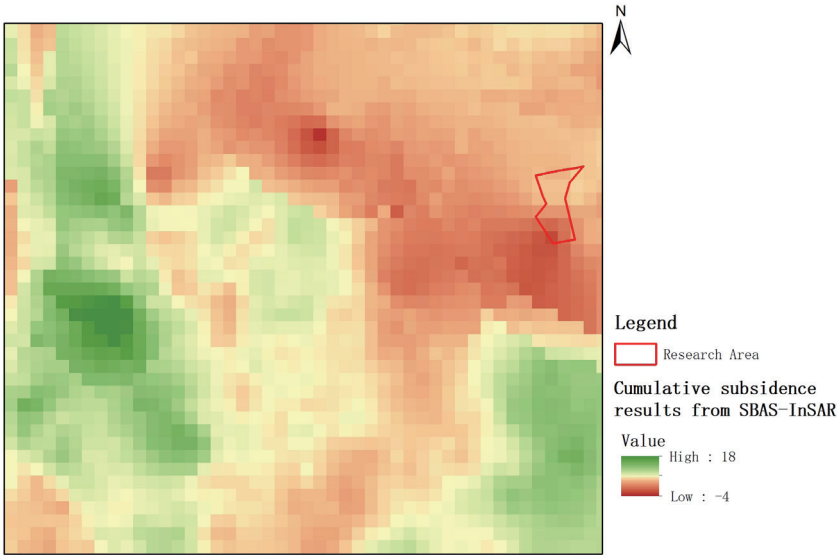

Fig. 8. (Color online) Cumulative subsidence results obtained using SBAS-InSAR.

(3) Deformation analysis: The deformation analysis by SBAS-InSAR is carried out using the data after adding observation points. The deformation trends and anomalies are analyzed.
(4) Result verification: Whether the deformation results obtained after adding observation points are more accurate and reliable is evaluated.

5. Analysis of Results

The cumulative settlement corresponding to the SBAS-InSAR time is obtained from the differential interference time of D-InSAR data processing. The results are shown in Fig. 9, with

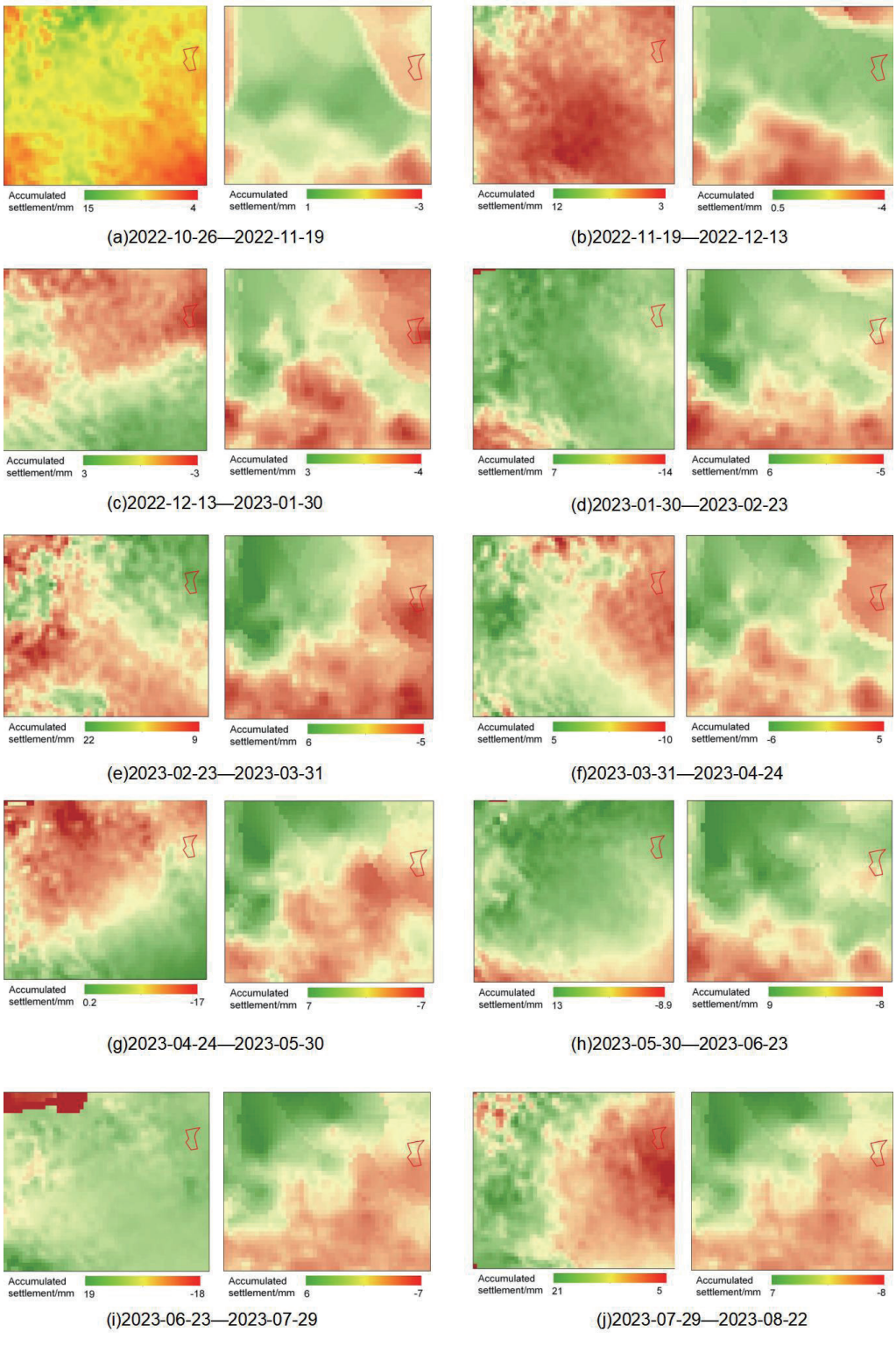

Fig. 9. (Color online) Cumulative subsidence of the study area at different stages.

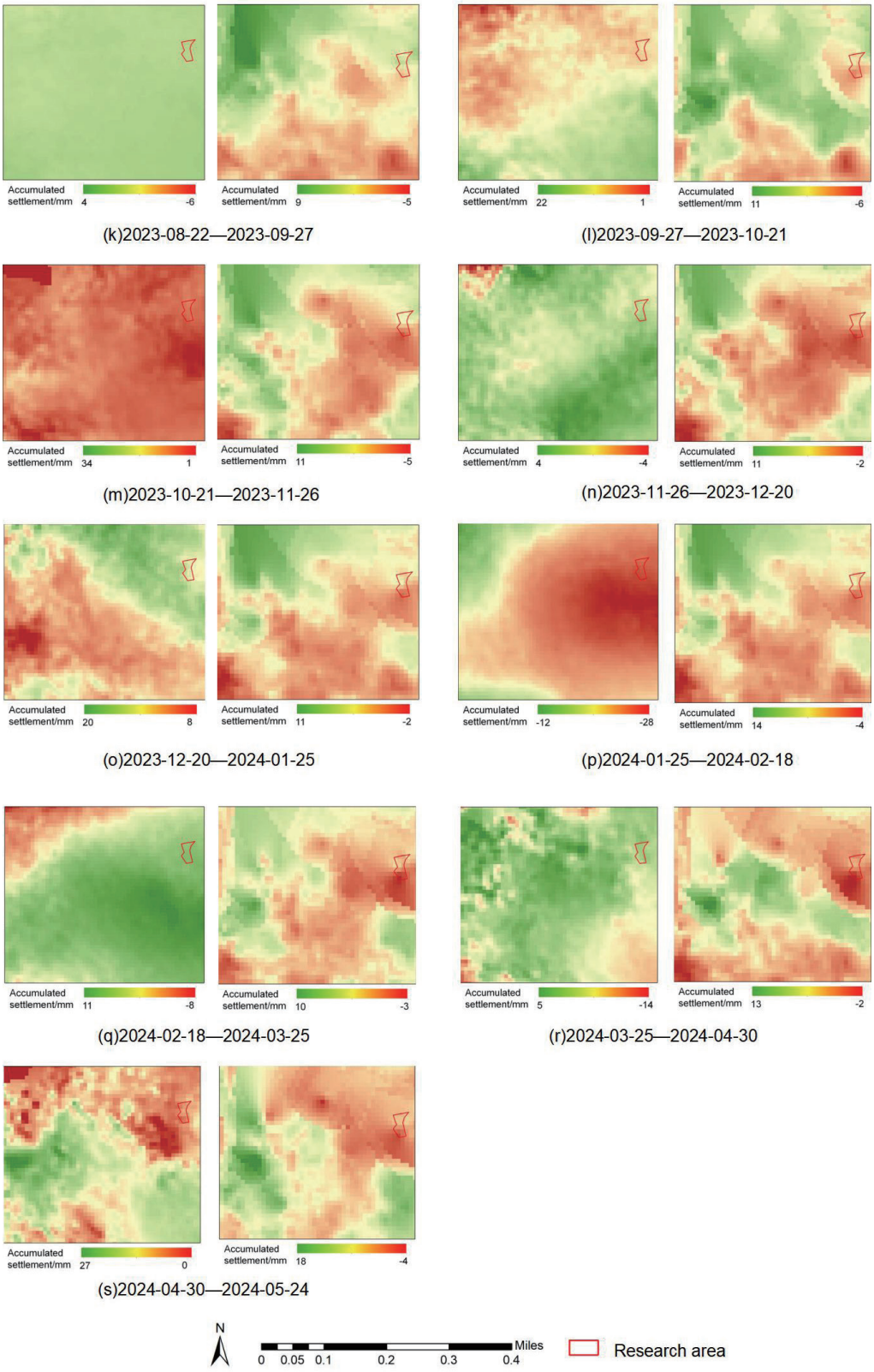

Fig. 9. (Color online) (Continued) Cumulative subsidence of the study area at different stages.

D-InSAR results on the left and SBAS-InSAR results on the right of each subgraph group. D-InSAR processes data independently in stages and calculates cumulative settlement through simple accumulation. This approach reflects the errors in each independent interferometric pair in the final cumulative settlement result. As shown in Fig. 9, this leads to significant errors and poor spatial continuity in the settlement region. In contrast, SBAS-InSAR uses time-series processing, which effectively removes atmospheric delay and other errors. The cumulative settlement results obtained with SBAS-InSAR have fewer errors and better spatial continuity. This improvement enhances the readability of settlement regions and supports the analysis of spatiotemporal evolution characteristics.

When the monitoring period is less than four months, the maximum cumulative displacement detected through SBAS-InSAR technology is generally greater than that detected by D-InSAR technology. However, as the monitoring duration increases, the maximum cumulative settlement measured with D-InSAR technology becomes significantly larger than that recorded and observed with SBAS-InSAR. By May 24, 2024, the maximum cumulative settlement in the study area reached 28 mm when using D-InSAR technology compared with only 8 mm when using SBAS-InSAR. The data processing in SBAS-InSAR uses a small baseline subset approach to generate a larger number of interferometric pairs with different spatial and temporal baselines. In the subsequent time series analysis, phase information from these overlapping interferometric pairs complements each other. This approach addresses a limitation of D-InSAR, which relies on individual interferometric pairs to extract phase information for specific time intervals. This advantage enables a more comprehensive understanding of surface subsidence and provides valuable insights into ground movement dynamics.

6. Conclusions

In this study, we analyzed land subsidence in cultivated farmland in the hilly area of a city, using 20 scenes of VV-polarized Sentinel-1A data collected between October 26, 2022 and May 24, 2024. We compared the results of using D-InSAR and SBAS-InSAR techniques to assess their relative performances.

(1) D-InSAR was revealed to detect a cumulative settlement of 28 mm, which is significantly higher than the 8 mm recorded by SBAS-InSAR. The discrepancy arises from D-InSAR's sensitivity to independent phase errors, which accumulate over time and compromise spatial continuity, reducing its reliability for long-term monitoring.
(2) SBAS-InSAR outperformed D-InSAR by mitigating atmospheric delay and noise through time-series processing. This approach enhanced spatial continuity and accuracy, making SBAS-InSAR more effective for monitoring deformation trends and spatiotemporal changes, particularly in hilly terrains.
(3) The results of this study underscore SBAS-InSAR's superiority for monitoring land subsidence in complex topographies. Its ability to maintain coherence and accuracy over extended periods highlights its potential for sustainable agricultural land monitoring, warranting further optimization, improved spatial resolution, and integration with other technologies.

Acknowledgments

The authors thank the National Natural Science Foundation of China (42171416) and the Research project on key technologies of cultivated land change and planting attribute monitoring in hilly regions (H24187).

References

1 E. Ni, J. Zhang, M. Qiu, L. Quan, and X. Zhu: Beijing Surv. Mapp. **38** (2024) 312. https://doi.org/10.19580/j.cnki.1007-3000.2024.03.007
2 Z. Yang: Guilin University of Electronic Technology (2023). https://doi.org/10.27049/d.cnki.ggldc.2023.001201
3 X. Zhou, P. Shi, J. Zhang, Z. Gao, and F. Guoe: Geospatial Inf. **22** (2024) 53.
4 Q. Zhu, L. Gu, X. Liu, Y. Yin, and S. Zhu: Metal Mines (2024) 1–11. http://kns.cnki.net/kcms/detail/34.1055.TD.20230807.1254.002.html
5 X. Xu, H. Mao, and L. Lan: Beijing Surv. Mapp. **37** (2023) 1308. https://doi.org/10.19580/j.cnki.1007-3000.2023.09.020.10.19580/j.cnki.1007-3000.2023.09.020
6 S. Wang and S. Wang: Surv. Spatial Geogr. Inf. **46** (2023) 178.
7 M. Guo, Y. Wei, Z. Chen, Y. Zhao, X. Tang, K. Guo, and K. Tang: Sens. Mater. **36** (2024) 3713. https://doi.org/10.18494/SAM4702
8 L. Ma, R. Cai, F. Zhang, and Q. Liu: Henan Sci. Technol. **51** (2024) 37. https://doi.org/10.19968/j.cnki.hnkj.1003-5168.2024.03.008
9 X. Yan, B. Feng, and W. Liu: Sci. Technol. Innovation **16** (2024) 62.
10 P. Wang, P. Cheng, and X. Wang: China Mining **33** (2024) 133.
11 M. Guo, Y. Zhou, T. Zhou, and D. Pan: Int. Arch. Photogramm. Remote Sens. Spatial Inf. Sci., XLIII-B2-2020 (2020) 1455–1463. https://doi.org/10.5194/isprs-archives-XLIII-B2-2020-1455-2020
12 Y. Shi, X. Zhe, Y. Zhang, K. Wang, K. Zhang, and R. Wu: J. Safety Environ. **24** (2024) 3429. https://doi.org/10.13637/j.issn.1009-6094.2023.2594
13 Z. Gu, Y. Dong, and F. Li: China Water Transport (Second Half) **24** (2024) 108.
14 X. Yang, T. Li, Y. Zhang, G. Zhang, and H. Liu: Mod. Coal Mines **33** (2024) 9. https://doi.org/10.13606/j.cnki.37-1205/td.2024.03.026
15 S. Wang, L. Zhang, J. Zhou, F. Zhang, Z. Han, and F. Yin: J. Eng. Geol. **31** (2023) 1951. https://doi.org/10.13544/J.cnki.jeg.2021-0050
16 Y. Jin, H. Hu, and Y. Cai: Coal Technol. **42** (2023) 30. https://doi.org/10.13301/j.cnki.ct.2023.11.006
17 D. Wei and S. Wang: Adv. Geophys. **39** (2024) 498.
18 S. Zhang and P. Zhao: Geol. Sci. **58** (2023) 1521.
19 D. Huang: East China Geol. **44** (2023) 476. https://doi.org/10.16788/j.hddz.32-1865/P.2023.04.011
20 W. Wu and J. Hu: Eng. Technol. Res. **8** (2023) 28. https://doi.org/10.19537/j.cnki.2096-2789.2023.16.009
21 Z. Liu, X. Sun, B. Wu, S. Zhu, and G. Xu: Coal Technol. 42 (2023) 192. https://doi.org/10.13301/j.cnki.ct.2023.06.044
22 M. Guo, X. Tang, Y. Liu, C. Wang, and Y. Wei: Optics Precis. Eng. **31** (2023) 1988. https://doi.org/10.37188/OPE.20233113.1988
23 J. Zhang: Shandong University of Science and Technology (2011). https://doi.org/10.7666/d.D300787
24 B. Xu and N. Shao: Geomatics Spatial Inf. Technol. **44** (2021) 175. https://doi.org/202110.3969/j.issn.1672-5867.2021.12.0472021